



AIAA 2002-06979

Accuracy of Measurements of Cloud
Ice Water Content by the Nevzorov Probe
Ice

Alexei V. Korolev and J. Walter Strapp
Meteorological Service of Canada
Downsview, Ontario, Canada

40th Aerospace Sciences Meeting & Exhibit
14–17 January 2002
Reno, Nevada

Accuracy of Measurements of Cloud Ice Water Content by the Nevzorov Probe

Alexei V. Korolev and J. Walter Strapp

Cloud Physics Research Division, Meteorological Service of Canada,
Downsview, Ontario, Canada

ABSTRACT

This article studies the accuracy of measurements of cloud ice water content (IWC) in glaciated clouds using the airborne Nevzorov LWC/TWC probe. The Nevzorov probe is a constant temperature hot-wire instrument for measurement of liquid water content (LWC) and total (ice+liquid) water content (TWC). IWC was calculated from measurements of TWC and LWC. The phase discriminating capability was tested in a wind tunnel using frozen sprays. The IWC measured in natural clouds by the Nevzorov probe was compared to that calculated from PMS OAP-2D images. It was found that IWC derived from the Nevzorov and OAP-2D imagery correlates well.

INTRODUCTION

Water in solid and liquid forms may be considered as one of the significant substances in the atmosphere affecting mobile platforms such as airplanes, helicopters, balloons, etc. Ice particles may affect the performance of aircraft engines or may even result in its icing (Riley¹ 1998). Most previous studies of condensed water in tropospheric clouds have focused on the characterization of its liquid fraction. During the past two decades, new developments in aircraft instrumentation have significantly improved the measurements of total (ice + liquid) water content (Nevzorov² 1980; Brown³ 1993; Twohy et al.⁴ 1997), allowing estimation of ice water content (IWC).

In this study, IWC was measured by the Nevzorov aircraft hot wire probe (Korolev et al.⁵ 1998). One of the past and current problems in measurements of IWC is the absence of calibration standards and calibrating techniques. One available method used here is to test the response of liquid and total water to frozen sprays in icing wind tunnels. In addition, comparisons of IWC derived from the Nevzorov and two-dimensional optical array probes (OAP-2D) suggest that under certain conditions IWC calculated from OAP-2D ice particle images may give reasonably accurate results.

INSTRUMENTATION

The Nevzorov probe is a constant temperature hot-wire instrument consisting of two sensors: (1) for measurement of LWC and (2) for TWC

(IWC+LWC), (Fig. 1). The Nevzorov LWC sensor has a cylindrical shape with a diameter of 2 mm. The Nevzorov TWC sensor is a concave cone, having a diameter of 8 mm, which works as a trap for impacting cloud particles. The threshold sensitivity to water and ice was estimated as $0.003\text{--}0.005\text{g m}^{-3}$. The questions related to the measurement accuracy of the Nevzorov probe were discussed in detail in Korolev et al.⁵ (1998).

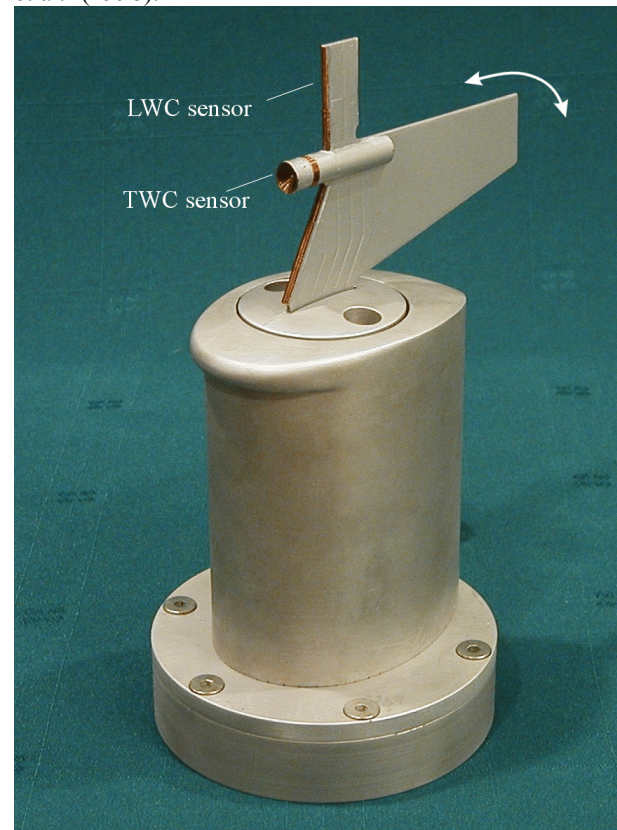


Figure 1: The Nevzorov LWC/TWC sensor head

The hydrometeor phase discrimination capability of the TWC and LWC sensors result from the expected difference in behaviour of liquid and solid particles impacting with their surfaces. Small liquid droplets, after collision with the LWC or TWC collector sensors are flattened into a thin surface film and completely evaporate. Ice particles tend to remain inside the conical hollow of the TWC collector until they melt and evaporate. In contrast, ice particles are expected to break away from the convex cylindrical surface of the LWC collector with negligible heat expended relative to that for complete ice evaporation.

The IWC and LWC can be derived from a system of equations described in Korolev et al.⁵ (1998)

$$W_{ice} = \frac{\epsilon_{iL}W_{TWC} - \epsilon_{iT}W_{LWC}}{\epsilon_{iL}\epsilon_{iT}k - \epsilon_{iT}\beta} \quad (1)$$

$$W_{liq} = \frac{\epsilon_{iT}k}{\epsilon_{iT}\epsilon_{iL}k - \epsilon_{iT}\beta} W_{LWC} - \frac{\beta}{\epsilon_{iT}\epsilon_{iL}k - \epsilon_{iT}\beta} W_{TWC} \quad (2)$$

where W_{TWC} and W_{LWC} are the uncorrected total and liquid water contents measured directly by the Nevzorov LWC and TWC sensors, respectively; ϵ_{iT} , ϵ_{iL} are the integrated collection efficiencies for liquid droplets and ice particles respectively for the TWC sensor; ϵ_{iL} is the integrated collection efficiency for liquid droplets for the LWC sensor; β is a coefficient accounting for the residual effect of ice particles on the LWC sensor; $k = L_i^*/L_l^*$ is a correction coefficient accounting for the difference between expended energy for water (L_l^*) and ice particle (L_i^*) evaporation.

The values of W_{TWC} and W_{LWC} were computed from instrument measurements as follows:

$$W_{TWC} = \frac{V_{TWC}^2}{UL_i^*S_{TWC}R_{TWC}} \quad (3)$$

$$W_{LWC} = \frac{V_{LWC}^2}{UL_l^*S_{LWC}R_{LWC}} \quad (4)$$

Here V_{TWC} and V_{LWC} are the voltages measured across the TWC and LWC sensors having the resistances R_{TWC} and R_{LWC} , respectively; S_{TWC} and S_{LWC} are sample areas of the TWC and LWC sensors, respectively, and U is the true air speed.

For liquid clouds, the specific energy expended in heating and evaporating can be written as:

$$L_l^* = C_l(T_e - T_a) + L_l(T_e) \quad (5)$$

where C_l is the specific heat of liquid water, T_a is the air temperature, $L_l(T_e)$ is the latent heat of

evaporation of water at the evaporation temperature T_e (Nevzorov⁶ 1983; Korolev et al.⁵ 1998).

For ice particles

$$L_i^* = C_i(T_0 - T_a) + L_i + C_i(T_e - T_0) + L_i(T_e) \quad (6)$$

where C_i is the specific heat of ice, L_i is the latent heat of melting, and $T_0 = 0^\circ\text{C}$.

For simplicity it is convenient to use an average value of $L_l^* = 2.58 \cdot 10^6$ J/kg and $L_i^* = 2.90 \cdot 10^6$ J/kg which adds a $\pm 5\%$ error to estimates of LWC and IWC for the typical range of water content for clouds with temperatures between -40°C and 0°C (Nevzorov⁶ 1983). Therefore, the coefficient $k = L_i^*/L_l^*$ in Eqs. 1 and 2 was assumed to be approximately equal to 1.12.

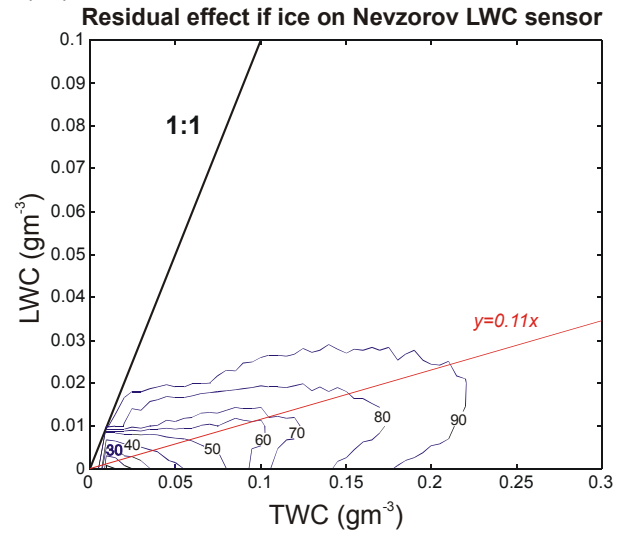


Figure 2. Scatter diagram of the Nevzorov LWC and TWC measurements in glaciated clouds. Contour lines indicate isopleths of probability for finding LWC and TWC inside the contour.

The residual effect of ice on the LWC sensor is due to the small amount of heat removed from the LWC sensor during collision with ice particles. The residual effect depends on size, shape and bulk density of ice particle, air speed, air temperature, and the temperature of the sensor.

The residual ice effect on the LWC sensor for the data set of this paper was estimated from Fig. 2, which shows a scatterplot of W_{LWC} versus W_{TWC} in glaciated clouds. The clouds were identified as glaciated if W_{TWC} exceeded a threshold value of $W_{thresh} = 0.005\text{g/m}^3$, and the ramp voltage (V_{RICE}) of the Goodrich Co. Rosemount Ice Detector (RICE) probe was not increasing, i.e.

$$W_{TWC} > W_{thresh} \quad (7)$$

$$dV_{RICE}/dt \leq 0. \quad (8)$$

Mazin et al.⁷ (2001) theoretically estimated the threshold sensitivity of the RICE probe as 0.006 g m^{-3} at 100 m s^{-1} . The threshold sensitivity for the RICE probe deduced from *in-situ* measurements was estimated as 0.01 g m^{-3} for a 30 second averaging time interval (Cober et al.⁸ 2001). The best-fit linear regression forced through the origin for the scatter diagram in Fig. 2 gives $W_{LWC}=0.11W_{TWC}$. From this result, we have estimated the coefficient $\beta=0.11$ in Eqs. 1 and 2. Similar results were shown by Cober et al.⁹ (2001) using 30-second averaged data.

It should be emphasised that the coefficient $\beta=0.11$ applies to air speeds typical for the Convair 580, i.e. $U \sim 100 \text{ m/s}$. The residual effect increases with an increase in aircraft speed and it may reach up to 50% of the indicated IWC at $U > 200 \text{ m s}^{-1}$ (Strapp et al.¹⁰ 1999).

In this study, the collection efficiencies ϵ_{IT} , ϵ_{IT} , ϵ_{IL} , for both LWC and TWC sensors in Eq. 1 and 2 were assumed to be equal to unity. For most liquid clouds without drizzle size droplets, the integrated collection efficiency for the LWC sensor ϵ_{IL} varies from 0.9 to 1 (Nevzorov⁶ 1983; Korolev et al.⁷ 1998). However, the liquid water content measured by the TWC sensor may be less than that measured by the LWC sensor by 20- 30% in small droplet clouds ($D < 5 \mu\text{m}$), due to the lower TWC sensor collection efficiency ϵ_{IT} . This may also be the case for small ice particles. However, with the exception of some special cases such as thunderstorm anvils (Strapp et al.¹⁰ 1999), for most clouds such as those described in this work the majority of IWC is contributed from particles with $D > 100 \mu\text{m}$, for which ϵ_{IT} to a good approximation is equal to 1. Based on the above considerations, Eqs. 1 and 2 can be rewritten as

$$W_{ice} = 0.99(W_{TWC} - W_{LWC}) \quad (9)$$

$$W_{liq} = 1.108W_{LWC} - 0.108W_{TWC} \quad (10)$$

Other relevant cloud microphysical instruments installed on the Convair-580, some of which are used in this study, include: two Rosemount temperature probes (BF Goodrich Aerospace Sensors Division*) and a reverse-flow temperature probe; a Cambridge EG&G dewpoint hygrometer; two PMS (Particle Measuring Systems) FSSP-100s (Forward Scattering Spectrometer Probe, Knollenberg¹¹, 1981), which measured droplet size distributions in two different size ranges of 2 - 32 μm and 5 - 95 μm ; two PMS King probes (King et al.¹² 1978); a Rosemount Icing Detector (BF Goodrich Aerospace Sensors Division*); a PMS OAP-2DC (25 - 800 μm); a PMS

OAP-2DC Gray (25 - 1600 μm); and a PMS OAP-2DP (200 - 6400 μm , Knollenberg¹¹, 1981). The three PMS OAP probes provided shadow images and concentrations of hydrometeors within their respective size ranges.

These instruments were installed on the National Research Council (NRC) Convair-580. The data from each instrument were carefully examined for indications of fogging and ice buildup. Cases with fogging or icing were excluded from consideration.

WIND TUNNEL TESTS

The response of the LWC and TWC sensors to ice particles was tested in the NRC Altitude Icing Wind Tunnel (AIWT). While maintaining a constant water spray, the temperature in the wind tunnel was decreased in a stepwise fashion (Fig. 3b), eventually producing a partial glaciation of the spray. Fig. 3a shows that the TWC stayed approximately constant while the LWC measured by the Nevzorov and King probes decreased with decreasing temperature as the spray glaciated in stages. The residual signal at cold temperatures is explained by the incomplete freezing of the spray and residual effect of ice on the liquid sensor. The presence of unfrozen water was confirmed by ice buildup observed on the sensor holders. This test demonstrates that the TWC sensor does indeed measure IWC content of sprays composed of small frozen droplets, and does suggest that the LWC sensor has only a small response under the same conditions, corroborating the basic principle of phase discrimination of the probe.

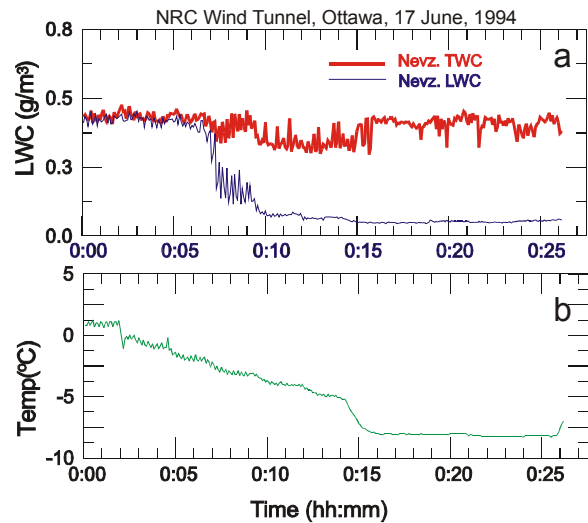


Figure 3. Response of the Nevzorov LWC and TWC sensors during glaciation of a constant condition spray in the NRC Altitude Icing Wind Tunnel.

* Formerly Rosemount Inc.

Further corroboration in ice particles more representative of natural cloud conditions has not been possible due to the lack of facilities capable of producing such conditions. However, Korolev et al.⁵ (1998) have provided further examples of the probe operation in natural clouds that demonstrate that it provides phase discrimination data that seem reasonable in the context of other data. Further evidence will be reported in this article, namely the high correlation between OAP-2D derived masses and IWC derived from the Nevzorov probe.

COMPARISON WITH OAP-2D DERIVED IWC

The IWC measured by the Nevzorov probe in glaciated clouds has been compared with that computed from OAP-2D images. Following Locatelli and Hobbs¹³ (1974) the mass of ice particles was calculated as

$$M = aD^b \quad (11)$$

where D is the size of the maximum dimension of an ice particle, and is defined differently by these authors according to ice particle type. Brown and Francis¹⁴ (1995) compared the mass derived from OAP-2D images, using the mass-diameter expression from Locatelli and Hobbs¹³ (1974) for aggregates of unrimed bullets, columns and side planes ($a=7.39 \times 10^{-11}$ and $b=1.9$), to that derived from their evaporative total water content system, and found that for two cirrus cases the agreement was quite reasonable. In Locatelli and Hobbs¹³ (1974), the maximum dimension was defined as the diameter of the smallest circle into which the aggregate as photographed could fit into without changing its density. In the case of Brown and Francis¹⁴ (1995), D was taken as the mean of maximum chord lengths measured in the parallel and perpendicular directions relative to the probe photodiode array.

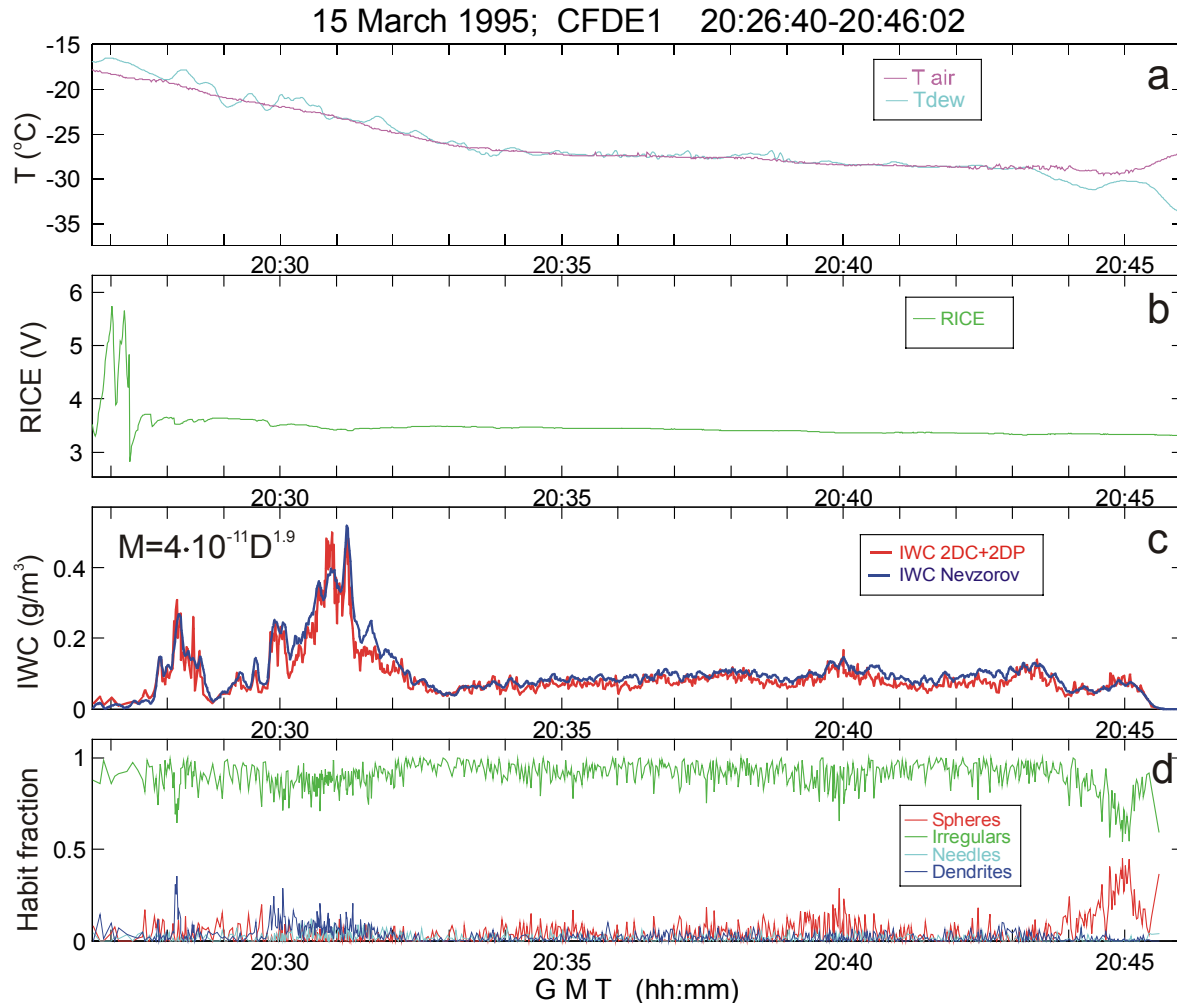


Figure 4. Time history of air and dew point temperature (a), RICE ramp signal (b), IWC measured by the Nevzorov probe and calculated from OAP-2DC and 2DP imagery for $a=4 \times 10^{-11}$ and $b=1.9$ in Eq. 11 (c), fraction of primary particle shape types of ice particles (d). Measurements were conducted in As-Ns, 15 March 1995, Newfoundland.

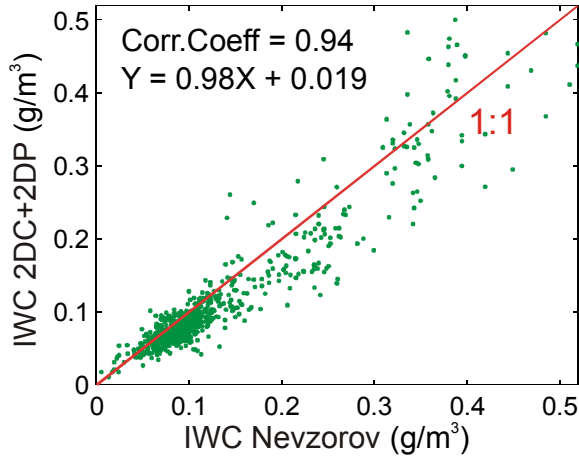


Figure 5 Scatterplot of I_N and I_{2D} for the case shown in Fig. 4

In the present study the dimension D was taken as the length of a ‘box’ circumscribing the image parallel to the probe photodiode array. For most cases it was

found that the best agreement with the Nevzorov IWC was found if the value of a was changed to between 3×10^{-11} and 5×10^{-11} . As in Brown and Francis¹⁴ (1995), small ice particles $D < 100 \mu\text{m}$ were treated as ice spheres ($a = 4.82 \cdot 10^{-13}$ and $b = 3$).

Figure 4 shows time histories of temperature (a), RICE ramp voltage (b), IWC measured by the Nevzorov probe I_N and that computed from the OAP-2D imagery I_{2D} (c), and the fraction of the primary shapes of cloud particles (d). The shapes of OAP-2DC images were classified using a recognition technique described in Korolev and Sussman¹⁵ (2000). The lack of activity of the RICE (Fig.4b), and results of the particle shape recognition analysis (Fig.4d) indicate that the measurements were conducted in mostly glaciated cloud. As seen from Fig. 4b, on the average I_N agrees well with I_{2D} calculated for $a = 4 \cdot 10^{-11}$ and $b = 1.9$. The scatter diagram in Fig. 5 shows high correlation (0.95) between I_N and I_{2D} .

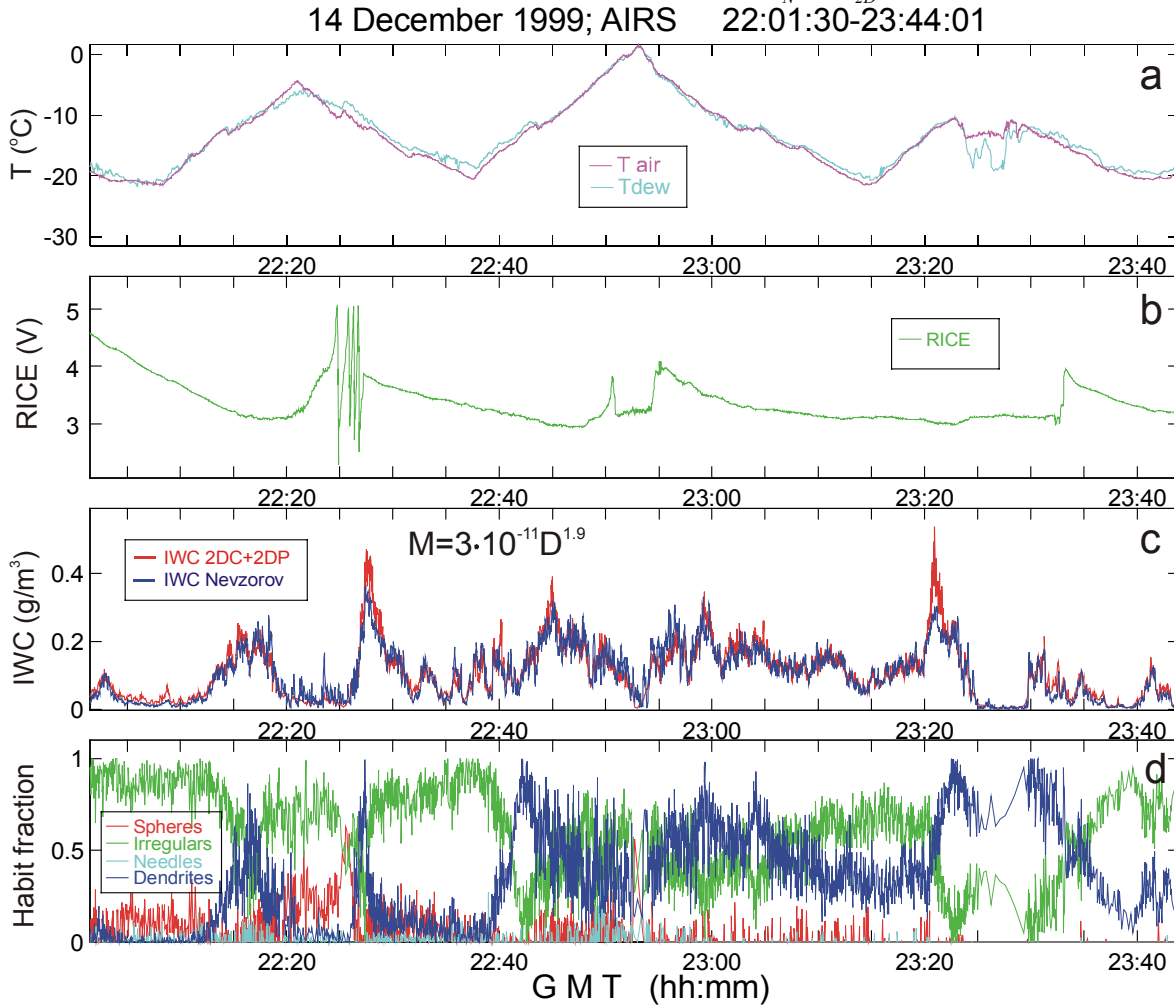


Figure 6. Same as in Fig 4. The I_{2D} was calculated for $a = 3 \times 10^{-11}$ and $b = 1.9$ in Eq. 11

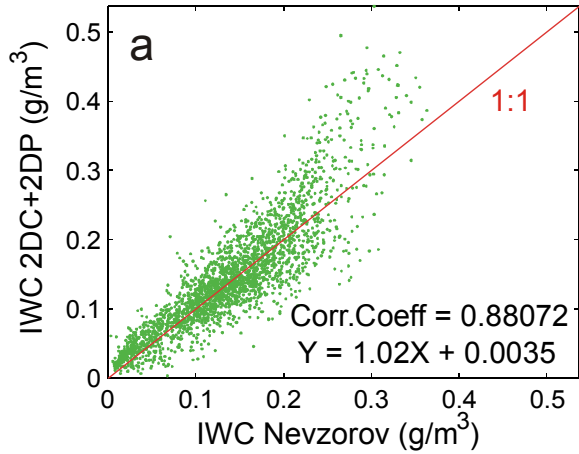


Figure 7 Scatterplot of I_N and I_{2D} for the case shown in Fig. 6

Another comparison of I_N and I_{2D} is shown in Fig. 6. Again, this case is characterized by only occasional activity on the ice detector (Fig. 6b), indicative of mostly glaciated conditions. The best-fit between I_N and I_{2D} as in the previous case is close to the one-to-one line (Fig. 8), although it was necessary to change the coefficient a in the calculation of I_{2D} to 3×10^{-11} to achieve this agreement. The most likely explanation for the requirement of different a coefficients in these two cases is a difference in average density of the ice particles, resulting from different atmospheric growth conditions that determine ice particle shapes densities. This is supported by differences in temperatures (Figs 4a and 7a), a primary factor in ice shape determination, and differences in the fractions of particle shape types (Figs 4d and 7d) observed in these two cases.

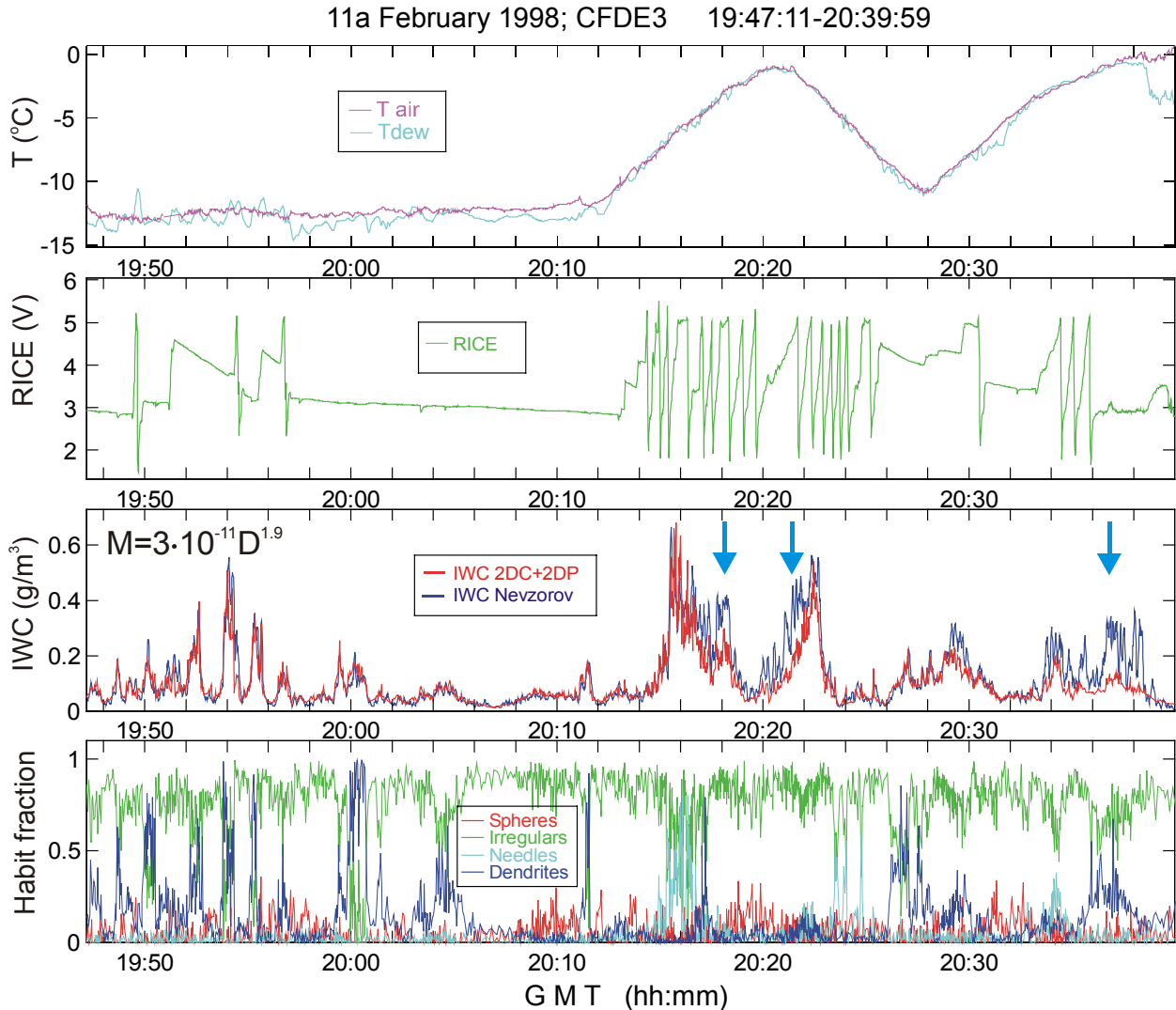


Figure 8. Same as in Fig 4. The I_{2D} was calculated for $a=3 \times 10^{-11}$ and $b=1.9$ in Eq. 11. Arrows indicate the cloud regions with a large difference between I_N and I_{2D} .

The comparison of these two cases is likely an indication of the lack of universal a and b coefficients in the size-to-mass parameterisation of Eq. 11. Figure 8 shows a time series similar to Fig. 4 and 7, but in this case the RICE signal indicates more frequent presence of liquid water. There are several cloud regions with large local differences between I_{2D} and I_N (illustrated by arrows), and where in neighbouring zones the I_{2D} estimate agrees with I_N . These regions are associated with, or close to regions of high liquid water content. The differences may be caused by heavy riming of ice particles, resulting in an increase in their density relative to neighbouring regions. If this were the case, the a coefficient chosen for the larger region would be inappropriate for the local region.

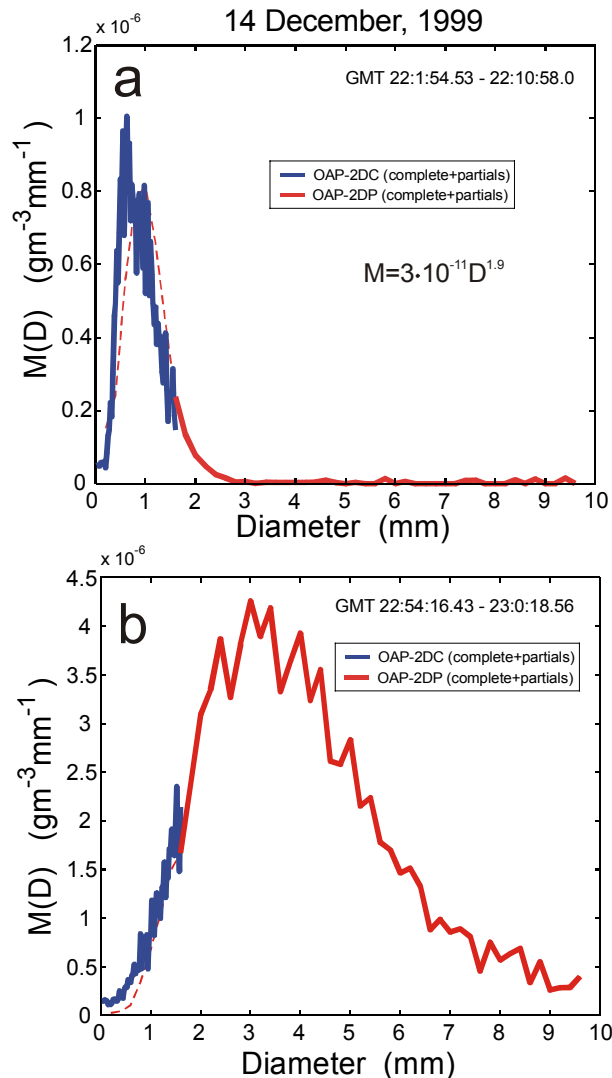


Figure 9 Size distributions calculated from OAP-2DC and OAP-2DP images for two selected cloud regions of Fig.6.

The I_{2D} was calculated for the range of particle sizes from $25\mu\text{m}$ to 9.8mm , as measured by PMS OAP-2DC ($25\text{-}800\mu\text{m}$) and OAP-2DP ($200\text{-}6000\mu\text{m}$). The sizes of partial images outside the nominal size range of the OAP probes were reconstructed using a technique suggested by Heymsfield and Parrish¹⁶ (1979).

It should be noted that significant IWC can be found through the upper size range of both the OAP-2DC and OAP-2DP probes. Using only one of these instruments may result in significant underestimation of IWC. Figure 9 shows mass distributions from combined from OAP-2DC and 2DP data for two selected time periods in Fig. 6. It is seen from Fig. 9b that disregarding by the 2DP data may result in large errors in IWC. A comparison of Figs. 9a and 9b reveals that the mass distributions can be expected to be concentrated in different size regions. In some special cases such as thunderstorm anvils, there is evidence that ice particle mass may even be concentrated below the practical detection limit of the OAP-2DC probe (Strapp et al.¹⁰ 1999). Note that there is insignificant mass in Figs. 9a and 9b in the variable depth-of-field region of the 2D-C below about $100\mu\text{m}$. Therefore sizing errors due to digitisation, time response, and out-of-focus images which are most important in this size region (Korolev et al.¹⁷ 1998, Strapp et al.¹⁸ 2001) are of minor significance in these two cases.

Boudala et al.¹⁹ (2001) have compared three different mass-diameter parameterisation schemes and concluded that OAP mass estimates on the average yielded scheme differences of up to 40%. Difference between individual cases within a single scheme were not discussed, although the significant scatter in their data reveals that such differences are significant, consistent with the results of this study.

CONCLUSIONS

The following results have been obtained in this study:

1. Frozen sprays in icing wind tunnels can be used to demonstrate the phase discrimination capability of the Nevzorov hot-wire TWC probe, and provide calibration verification for small frozen ice spheres.
2. Ice water content derived from OAP-2D imagery using a Locatelli and Hobbs¹³ (1974) size-to-mass conversion ($M = aD^b$) correlates very well with IWC measured by the Nevzorov probe. The best coefficients in the size-diameter relationship varied

from case to case. The best agreement between I_{2D} and I_N was found for coefficient values of $a=4 \times 10^{-11} \pm 1 \times 10^{-11}$ and $b=1.9$. These coefficients yield ice masses roughly half of those found to provide the best agreement in the comparisons of Brown and Francis¹⁴ (1995) for two cirrus cases.

3. The data presented in this study indicate that due to natural variability of ice particle shapes and bulk densities there is no universal set of a and b coefficients to characterize all clouds. These coefficients must be estimated for each situation individually, based on bulk IWC comparisons with another instrument such as the Nevzorov hot-wire probe.

REFERENCES

1. Riley, R.K., 1998: Mixed-phase icing conditions: A review. U.S. Dept. of Transportation Report DOT/FAA/AR/98/76, 45pp.
2. Nevzorov, A. N. 1980: Aircraft cloud water content meter. *Comm. a la 8eme conf int. sur la phys. des nuages, Clermont-Ferrand, France*, v. II, 701-703.
3. Brown, P.A. 1993: Measurements of the ice water content in cirrus using an evaporative technique. *J. Atmos. Oceanic Technol.*, **2**, 340-352.
4. Twohy C. H., Schanot, A. J. and Cooper W. A. 1997: Measurement of condensed water content and ice clouds using an airborne counterflow virtual impactor. *J. Atmos. Oceanic Technol.*, **14**, 197-202.
5. Korolev, A.V., Strapp, J.W. Isaac, G.A. and Nevzorov, A.N. 1998: The Nevzorov airborne hot-wire LWC-TWC probe: principle of operation and performance characteristics. *J. Atmos. Oceanic Technol.* **15**, 1495-1510.
6. Nevzorov, A. N. 1983: Aircraft cloud water content meter. *Transactions of Central Aerological Observatory (Trudi TsAO)*, 147, 19-26
7. Mazin, I. P., A.V. Korolev, A. Heymsfield, G. A. Isaac, and S. G. Cober, 2001: Thermodynamics of icing cylinder for measurements of liquid water content in supercooled clouds. *J. Atmos. Oceanic Technol.*, **18**, 543-558.
8. Cober, S.G., Isaac, G.A. Korolev, A.V. 2001: Assessing the Rosemount Icing Detector with in situ measurements. *J. Atmos. Oceanic Technol.*, **18**, 515-528.
9. Cober, S.G., Isaac, G.A. Korolev, A.V. and Strapp, J.W. 2001: Assessing cloud phase conditions. *J. Appl. Meteor.*, **40**, 1967-1983
10. Strapp, J.W., Chow, P. Moltby, M. Beezer, A.D. Korolev, A.V. Stronberg, I. and Hallett, J. 1999: Cloud microphysical measurements in thunderstorm outflow regions during Allied/BAE 1997 flight trials. *AIAA 37th Aerospace Sci. Meeting and Exhibit*, Reno, Nevada, 11-14 January 1999, AIAA 99-0498, pp10.
11. Knollenberg, R. G. 1981: Techniques for probing cloud microstructure. In: *Clouds, their formation, Optical properties, and Effects*, P. V Hobbs, A. Deepak, Eds. Academic Press, 495 pp.
12. King, W. D., Parkin D. A. and Handsworth, R. J. 1978 A hot-wire water device having fully calculable response characteristics. *J. Appl. Meteor.*, **17**, 1809-1813
13. Locatelli, J.D., and P.V. Hobbs, 1974: Fallspeeds and masses of solid precipitation particles. *J. Geophys. Res.*, **79**, 2185-2197.
14. Brown, P.R.A., and P.N. Francis, 1995: Improved Measurements of the Ice Water Content in Cirrus Using a Total-Water Probe. *J. Atmos. Oceanic Technol.* **12**, 410-414
15. Korolev, A. and Sussman, B. 2000: A technique for habit classification of cloud particles. *J. Atmos. Oceanic Technol.* **17**, 1048-1057.
16. Heymsfield, A.J. and Parrish, J. 1979: A computational technique for increasing the effective sampling volume of the PMS two-dimensional particle size spectrometer. *J. Appl. Meteor.*, **17**, 1566-1572
17. Korolev, A.V., J.W. Strapp, and G.A. Isaac, 1998: Evaluation of the accuracy of PMS optical array probes. *J. Atmos. Oceanic Technol.*, **15**, 708-720.
18. Strapp, J.W., F. Albers, A. Reuter, A.V. Korolev, U. Maixner, E. Rashke, and Z. Vukovic, 2001: Laboratory Measurements of the Response of a PMS OAP-2DC. *J. Atmos. Oceanic Technol.*, **18**, 1150-1170.
19. Boudala, F.S., G.A. Isaac, Q. Fu. and S.G. Cober, 2001: Parameterization of ice particle sizes for high latitude ice clouds. Accepted to *International. J. Climatology*